Enhancing the Open-Circuit Voltage of Molecular Photovoltaics Using Oxidized Au Nanocrystals

Lara-Jane Pegg, Stefan Schumann, and Ross A. Hatton*

Department of Chemistry, University of Warwick, Coventry, England, CV4 7AL

ARTICLE

ABSTRACT For organic photovoltaics (OPV) to realize applications effective strategies to maximize the open-circuit voltage must be developed. Herein we show that solution-processed surface-oxidized Au nanocrystals (o-AuNC) dramatically increase the open-circuit voltage (V_{oc}) of OPV cells based on boron-subphthalocyanine chloride (SubPc)/C_{60} and chloro-aluminum phthalocyanine (ClAlPc)/C_{60} heterojunctions when incorporated at the interface between the hole-extracting electrode and the phthalocyanine donor layer. In addition, the cell-to-cell variation in V_{oc} is reduced by up to 10-fold combined with a large reduction in the light intensity dependence of V_{oc}, both of which are important advantages for practical application. The largest increase in V_{oc} is achieved for SubPc/C_{60}-based cells which exhibit a 45% increase to 1.09 ± 0.01 V—an exceptionally high value for a single junction small molecule OPV. Remarkably these improvements are achieved using submonolayers of o-AuNC, which can be rationalized in terms of the exceptionally high work function of o-AuNC (~5.9 eV) and geometric electric field enhancement effects.

KEYWORDS: organic photovoltaics · organic solar cells · open-circuit voltage · gold nanoparticle · gold nanocrystal · electrode

Photovoltaics (PV) based on heterojunctions between small molecule[1] or polymeric[2] semiconductors have strong potential as a low cost, sustainable means of converting sunlight directly into electrical energy particularly for applications requiring power at the point of use. In these devices excitons are dissociated at the interface between donor- and acceptor-type light harvesting organic semiconductors generating free charge carriers which can be extracted to the external circuit under the influence of a built-in electric field and/or gradient in carrier concentrations.[3] The power conversion efficiency (η) of PV devices is directly proportional to the product of the short-circuit current density (J_{sc}), the voltage at the open-circuit condition (V_{oc}) and the fill-factor (FF). The latter is defined as the ratio $V_m J_m/(J_{sc}V_{oc})$ where V_m and J_m are the voltage and current at the maximum power-point. Since the first demonstration of a heterojunction organic photovoltaic (OPV) by Tang,[4] in which the heterojunction comprised a bilayer of donor- and acceptor-type organic semiconductors, a number of strategies have been developed to improve the η including (i) careful selection of the heterojunction materials to maximize light absorption[5,6] and the open-circuit voltage;[7] (ii) the introduction of additional layers to facilitate charge carrier extraction[8,9] and prevent exciton recombination at the electrodes; (iii) and the realization of complex interpenetrating heterojunctions (*i.e.*, bulk heterojunctions) to circumvent the restriction on photoactive layer thicknesses in bilayer OPV imposed by the short exciton diffusion length in organic semiconductors.[1] While the highest reported η in a single junction OPV to date has been achieved in a solution processed bulk-heterojunction OPV,[2] OPV cells based on vacuum deposited small molecules have also achieved promising performance.[1] Vacuum deposition is particularly well suited to the fabrication of multijunction OPV which offer a viable path to achieving $\eta \geq 10\%$, widely regarded as the threshold for market entry.[10] Of the three device parameters that determine η the origin of the V_{oc} in OPV is the least well understood, particularly as to the role of the electrodes,[1,11,12] and so widely applicable strategies to maximize V_{oc} are only just beginning to emerge.[8,13,14] At the same time it is clear that for device applications high voltage OPV are essential, not only to maximize η but also to minimize the number of cells that must be connected in series to deliver useful voltages.

In recent years chemically synthesized Ag and Au nanocrystals (AgNC and AuNC, respectively) have attracted attention as versatile materials for a host of applications.[15] In the context of OPV research, several research groups have incorporated

*Address correspondence to ross.hatton@warwick.ac.uk.

Received for review June 7, 2010 and accepted September 27, 2010.

Published online October 5, 2010. 10.1021/nn101276z

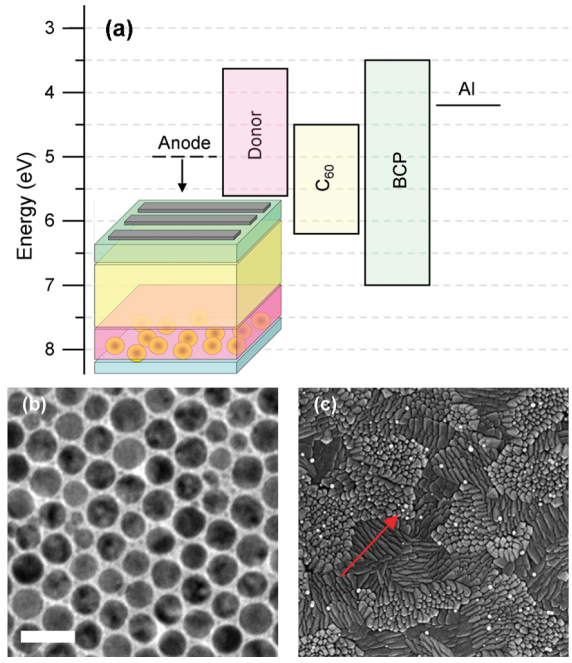

Figure 1. (a) Representation of OPV structure showing o-AuNC incorporated at the ITO/donor interface and a schematic energy level diagram for a donor/C_{60} OPV cell; (b) TEM micrograph of drop-cast OAm−AuNC; (c) FE-SEM micrograph of spin-cast OAm−AuNC on ITO glass. This image is representative of the lowest density utilized in this study. The scale bar corresponds to 20 and 200 nm for panels b and c, respectively.

chemically synthesized AuNC into solution processed OPV to enhance the light harvesting capability *via* plasmon enhanced absorption.[16,17] Previously, vacuum-deposited Ag nanoparticles had been utilized for this application,[18] although chemically synthesized NCs offer the important advantages of superior size and shape control combined with the possibility of derivatizing the NC surface with functional ligands. These reports have demonstrated the potential of plasmonic effects to deliver improvements in J_{sc} and FF of up to 10%, although in all cases V_{oc} was unchanged. In this work we have incorporated submonolayers of ~11 nm diameter surface-oxidized AuNC (o-AuNC) at the interface between the indium−tin oxide (ITO) transparent electrode and the donor layer in vacuum-deposited small molecule OPV (Figure 1a) to dramatic effect on V_{oc}. In addition to a large increase in V_{oc}, which translates into a commensurate increase in η, the dependence of V_{oc} on light intensity at low light levels is reduced and the cell-to-cell variation in V_{oc} is reduced by up to 10-fold. The latter is particularly important for practical applications since OPV must operate efficiently at low light levels and the performance characteristics of individual cells must be closely matched to minimize losses when assembling PV modules. To demonstrate the generality of this effect o-AuNC are incorporated into OPV employing donor materials which have significantly different ionization potentials (I_p), namely, SubPc I_p = 5.6 eV[19,20] and aluminum phthalocyanine chloride (ClAlPc), I_p = 5.3−5.4 eV,[5,20] and cell performance is correlated with o-AuNC surface density. Compelling evidence is presented that this improvement can be attributed to an increase in built-in electric field strength, which is remarkable because the density of o-AuNC required to achieve this improvement is submonolayer. To the best of our knowledge this is the first report of its kind and demonstrates the potential of o-AuNC as a versatile, solution-processed nanomaterial for small molecule PV applications.

RESULTS AND DISCUSSION

Oleylamine (OAm) capped AuNC (OAm−AuNC) were synthesized by the reduction of $HAuCl_4$ in OAm in the presence of oleic acid (OA) according to an adaptation of the method of Wang *et al.*[21] Unlike the reactants, OAm−AuNC are insoluble in alcohols rendering them amenable to purification by repeated washing in ethanol and centrifugation. For application in OPV the purified OAm−AuNC were dried and redispersed at known concentration in toluene. Light scattering measurements and transmission electron microscope (TEM) imaging of purified OAm−AuNC verify that they were highly monodisperse with a diameter 11.4 nm ±1 nm. The tendency of these OAm−AuNC to assemble into two-dimensional hexagonally close-packed arrays separated by a constant interparticle distance of ~1.5 nm is characteristic of OAm-capped NC with a tight size distribution.[22]

Submonolayers of OAm−AuNC were spin-cast onto cleaned ITO glass substrates from toluene solutions and UV/O_3 treated immediately prior to device fabrication. Details of the solvent cleaning procedure are given in the experimental section. Unless otherwise stated, ITO glass substrates for reference cells were treated in an identical way without OAm−AuNC deposition. Surface oxidative treatments such as UV/O_3 are widely used to remove residual carbon from solvent cleaned ITO glass prior to fabricating OPV.[8,13,23] However, very little is known about the effect of UV/O_3 treatment on alkyl-capped AuNC, beyond a study by Pang *et al.*[24] in which it is shown that UV/O_3 is an effective means of removing the alkyl chains from the upper most surface of alkyl-capped AuNC while leaving the ligand on the underside intact. We have investigated the final chemical state and work function of 11.4 nm OAm−AuNC after UV/O_3 treatment using core level electron spectroscopy (X-ray photoelectron spectroscopy, XPS) and contact potential measurements (Kelvin probe). Measurements were made on both continuous AuNC films and submonolayer AuNC coverage on ITO glass. Details of the UV/O_3 treatment are given in the experimental section of this paper. High resolution XPS spectra of the Au 4*f* region of OAm−AuNC before and after UV/O_3 treatment provide compelling evidence for the formation of Au_2O_3 at the NC surface (Figure 2). The doublet at 87.3 and 83.6 eV is assigned to Au^0 $4f_{5/2}$ and

Au^0 $4f_{7/2}$, respectively (Figure 2a). Support for this assignment comes from comparison with the XPS spectra of an Au film measured in our laboratory and by a number of other researchers.[25,26] Upon UV/O_3 treatment a new doublet appears at ~1.9 eV higher binding energy which, based on literature values for the binding energy of 4f electrons in Au^{3+}, can be assigned to Au_2O_3.[25−27] To estimate the extent of oxidation of isolated OAm−AuNC on ITO, the XPS experiment was repeated on submonolayers of OAm−AuNC on ITO glass (Figure 2b), from which it is clear that the OAm−AuNC are only partially oxidized. King has previously shown that UV/O_3 of Au films for 1 h results in the formation of a ~1.7 nm oxide surface layer which prevents further oxidation.[25] Using the relative Au4f peak intensities in Figure 2b, an estimate of the mean free path of electrons in Au_2O_3 (3.1 nm)[28] and accounting for the size and shape of the o-AuNC[29] the oxide layer thickness is estimated to be ≤1 nm (Supporting Information). In view of the shorter oxidation time this result is consistent with the result of King.[25] Crucially 1 nm is not sufficient to impede electron transfer into the donor HOMO (*i.e.*, hole extraction); indeed, the functionality of Au films as a hole-injecting electrode in organic electronics is greatly improved upon surface oxidation.[27,30−32] To support the XPS measurements the work function of continuous films of OAm−AuNC before and after UV/O_3 treatment was measured using a Kelvin probe referenced to freshly cleaved graphite. The work function of the archetypal hole-extraction material poly(3,4-ethylenedioxythiophene):poly(styrenesulfonate) (PEDOT:PSS) was measured to be 5.0−5.1 eV in agreement with the literature.[12] The work function of OAm−AuNC was dramatically increased from 4.6 ± 0.15 to 5.9 ± 0.20 eV, which is significantly higher than that of pristine Au films (~5.2 eV).[27] This very high work function is also slightly higher than that reported by Rentenberger *et al.*[27] for UV/O_3 films measured using ultraviolet photoelectron spectroscopy (UPS): ~ 5.5 eV, which can be attribute to size effect[33,34] and/or the difference in the measurement technique used, since UPS measures the lowest work function.

Figures 3 and 4 show that incorporation of o-AuNC at the ITO/donor interface dramatically increases the η of cells employing SubPc or ClAlPc as the donor material. This improvement results from an increase in V_{oc} only, with no significant change in J_{sc} or FF. The V_{oc} in both cell structures is higher than that achieved using the archetypal hole extraction layer PEDOT:PSS: SubPc 0.80 V (Supporting Information, Figure S1) and ClAlPc 0.72 V,[20] and, in the case of cells employing SubPc (1.09 V ± 0.01 V), is equal to the highest reported for any single junction small-molecule OPV.[35] Furthermore, in both cases the increases in V_{oc} are accompanied by a dramatic reduction in the cell-to-cell variation in V_{oc} by as much as10-fold. Remarkably, these improvements are achieved for submonolayer coverage of o-AuNC,

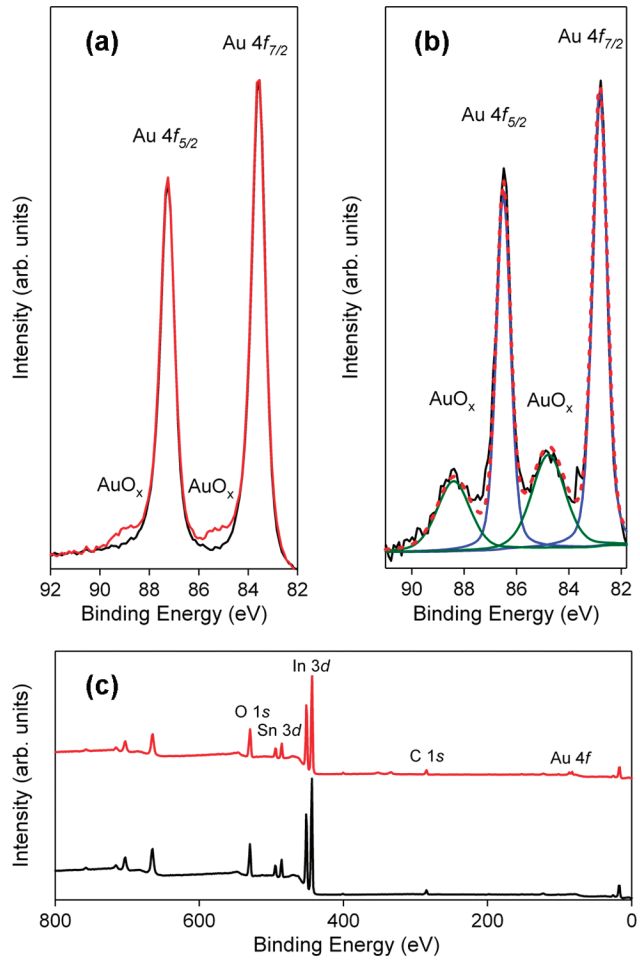

Figure 2. (a) High resolution XPS spectra of the Au 4f region for dense OAm−AuNC films on ITO glass before (black) and after (red) UV/O_3 treatment.; (b) Au 4f region—with peak fitting—for a submonolayer OAm−AuNC film on ITO glass after UV/O_3 treatment; (c) representative XPS survey spectra for a submonolayer film of UV/O_3 treated OAm−AuNC on ITO glass (red) and ITO glass reference solvent cleaned and UV/O_3 treated in an identical way (black).

with the increase in V_{oc} beginning to saturate for surface densities of only ~150 o-AuNC per μm^2 (Figure 1c).

The absence of a statistically significant increase in J_{sc} and associated modification of the shape of the incident-photon-to-electron-conversion-efficiency (IPCE) spectra (Supporting Information, Figure S2.) shows that plasmon-enhanced light absorption does not play a significant role for the o-AuNC loadings utilized in this study. Notably, the o-AuNC density required to achieve the large increase in V_{oc} reported herein is significantly higher than the optimal surface density for plasmon-enhanced light absorption reported by Chen *et al.*[16] and Lee *et al.*[17]

A number of control experiments were performed to investigate the possibility that the increase in V_{oc} stems from low levels of impurities at the ITO/donor interface, originating either from the OAm−AuNC synthesis or solvent used to spin-cast the OAm−AuNC: (i) High resolution XPS of ITO glass substrates with and without submonolayers of o-AuNC show that the per-

centages of elements other than Au, namely O, In, Sn, Cl, C, and N are identical. For example, Figure 2c shows a survey scan taken of a monolayer film spun from OAm−AuNC solution 50% more concentrated than used in OPV cells (*i.e.*, 12 mg mL^{-1}) in order to maximize the likelihood of detecting low level impurities. This result is compelling evidence that the increase in V_{oc} does not result from differences in the levels of impurities at the ITO/donor interface. Furthermore the comparable levels of Cl measured using XPS are consistent with the results of inductively coupled plasma mass spectroscopy analysis of the purified OAm−AuNC solutions in toluene as compared to analytical grade toluene (<1 ppm). (ii) Control OPV cells utilizing ITO spin-coated with toluene and UV/O_3-treated exhibited the same V_{oc} as cells without toluene treatment (*i.e.*, as the reference cells) ruling out the possibility that the increase in V_{oc} could be attributed to impurities derived from the toluene. Crucially, without UV/O_3 treatment the performance of cells with and without OAm−AuNC was also comparable to the reference cells (Supporting Information, Figure S1). Thus without UV/O_3 treatment OAm−AuNC does not operate to increase V_{oc} proving that the oxide at the surface of o-AuNC plays a critical role in determining the functionality. (iii) Finally, cells were fabricated on ITO glass substrates spin-cast with dilute solutions (1×10^{-4} M) of the OAm, OA, and 1:1 OAm:OA followed by UV/O_3 treatment, since these materials were used to synthesize the OAm−AuNC. Again the V_{oc} was comparable to that of reference cells. Collectively this set of control experiments rules out the possibility that the increase in V_{oc} results from low levels of impurities at the ITO/donor interface, originating either from the OAm−AuNC synthesis or solvent used to spin-cast the OAm−AuNC.

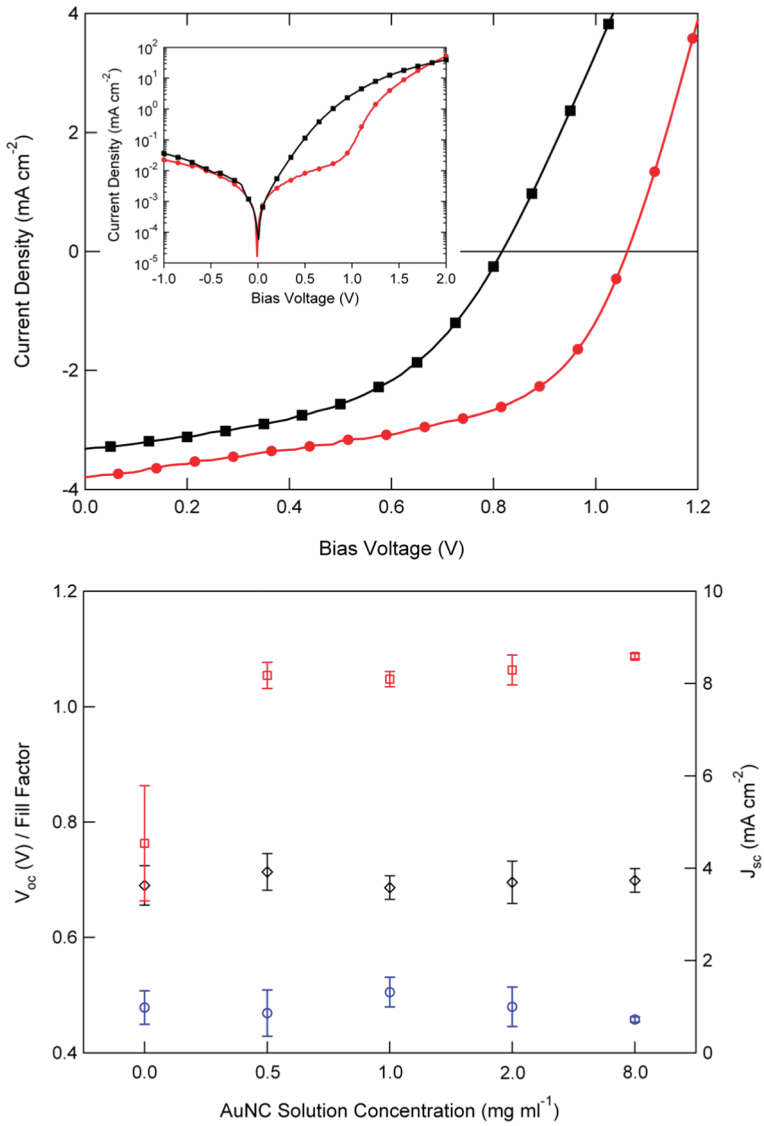

Figure 3. (Top) Representative *J*−*V* characteristics for a SubPc/C_{60} device under 1 sun illumination for ITO-only (black) and o-AuNC-modified ITO (red). Representative dark-current characteristics are given in the inset. (Bottom) Summary of key device characteristics as a function of o-AuNC loading: V_{oc} (red squares); J_{sc}, (black diamonds); FF (blue circles).

To rationalize the increase in V_{oc} upon incorporation of o-AuNC, it is necessary to consider the factors that determine V_{oc} in bilayer OPV. V_{oc} is the voltage across a cell under illumination when the photocurrent (J_{ph}) is exactly offset by the dark current (J_d) and has a maximum value given by the difference in energy between the donor I_p and acceptor electron affinity minus the binding energy of the dissociated geminate pair.[36] This offset is largest in cells utilizing SubPc as the electron donor owing to its larger I_p[20] as compared to ClAlPc, and so cells utilizing SubPc exhibit the largest V_{oc}. For a given photoactive heterojunction there are two contributions to the measured V_{oc} in bilayer OPV:[3,36,37](i) V_{oc} scales with the difference in the built-in potential (V_{bi}), given by the difference in work function between the two electrodes, once interfacial effects have been taken account; (ii) an intensity dependent contribution which is related to processes at the heterojunction rather than the electrodes. The latter has its origin in the diffusion current resulting from the asymmetry in cell structure, which is exactly offset by a forward drift current at V_{oc}. As a result of the latter, V_{oc} in bilayer OPV can significantly exceed the V_{bi} when the

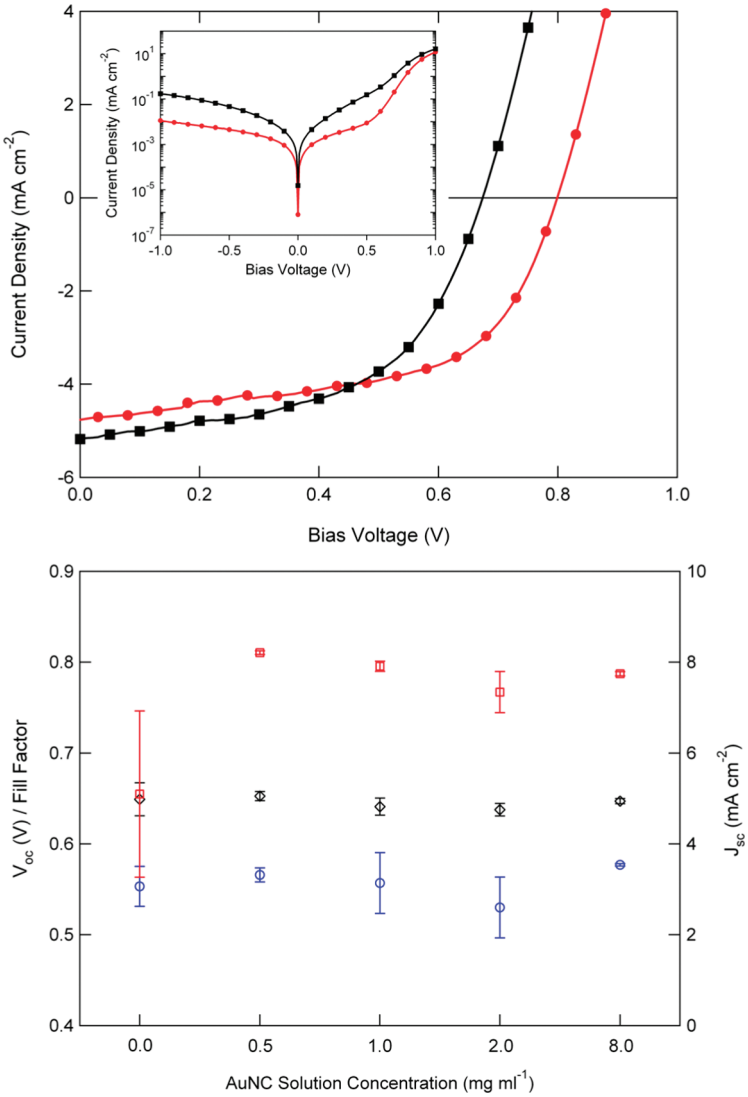

Figure 4. Representative *J*−*V* characteristics for a ClAlPc/C_{60} device under 1 sun illumination for ITO-only (black) and o-AuNC modified ITO (red). Typical dark-current characteristics are given in the inset. (Bottom) Summary of key device characteristics as a function of o-AuNC loading: V_{oc} (red squares); J_{sc}, (black diamonds); FF (blue circles).

Fermi level of each electrode is not closely aligned to the relevant frontier molecular orbitals in the adjacent organic semiconductor layer.

To date two strategies for increasing the V_{oc} in OPV have been proposed. The first is the introduction of an electron blocking layer at the interface between the hole-extracting electrode and the photoactive heterojunction to impede electron leakage current.[8,13] The effect of this modification is to suppress the dark current under forward bias such that photocurrent is not offset by the dark current (which flows in the opposite direction) until higher *V*. This modification also increases the Schottky barrier height to electron-injection in reverse bias, and so the reverse dark current is also reduced. The second approach is to increase the V_{bi} by increasing the work function of the hole-extracting electrode (and/or reducing the work function of the electron extracting electrode) to improve alignment between the electrode Fermi level and the relevant frontier molecular orbital in the adjacent molecular semiconductor.[14] This modification delays the onset of the sharp rise in forward dark current because a greater V_{bi} must be compensated. In this case the effect on the reverse dark current of increasing the V_{bi} is analogous to that of the electron blocking layer since the Schottky barrier height to electron injection in reverse bias is increased. It is clear from the insets in Figure 3 and 4 that the reason for the increase in V_{oc} in cells incorporating o-AuNC is the delay in the sharp rise in dark current under forward bias. A plausible explanation for this is an increase in the V_{bi} upon incorporation of o-AuNC, since the work function of o-AuNC (~5.9 eV) is significantly larger than that of UV/O_3-treated ITO glass (~5.6 eV) and very much larger than OAm−AuNC (~4.6 eV). However, without detailed knowledge of interfacial energetics at the contact with the donor material in each case, it cannot be assumed that the difference in work function would translate into a commensurate increase in built-in field.[38]

The large reduction in the variation in V_{oc} is evidence that the nature of the hole-extracting electrode is dramatically altered upon incorporation of o-AuNC. Evidence to support the conclusion that the increase in V_{oc} results from an increase in V_{bi} is provided by the light intensity dependence of V_{oc} in cells utilizing SubPc as the electron donor, since this OPV system exhibits the largest change in V_{oc} (Figure 5). At low light intensity cells with and without o-AuNC cells exhibit a logarithmic dependence of V_{oc} with incident light intensity, before saturating for intensities above 70 mW cm^{-2} (Figure 5). This can be understood in terms of the model proposed by Barker *et al.* for the operation of bilayer OPVs, in which at low light intensity and *V* greater than the V_{bi}, V_{oc} is determined by the competition between the diffusion driven photocurrent and the injected drift current.[36] However, when the electrode Fermi levels are optimally aligned with the relevant frontier molecular orbitals in the adjacent organic semiconductor, the light intensity dependence of V_{oc} will be weak, since V_{bi} is very close to the maximum attainable V_{oc} determined by the photoactive ma-

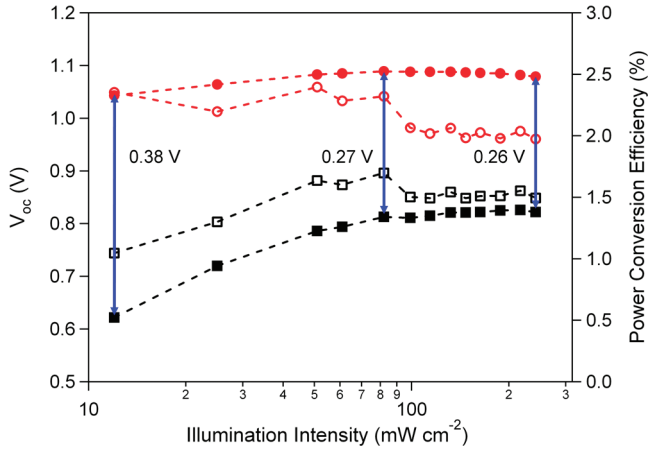

Figure 5. The effect of illumination intensity on V_{oc} (closed markers) and η (open markers) for ITO-only cells (black) and o-AuNC/ITO cells (red).

terial system. It is clear from Figure 5 that cells incorporating o-AuNC exhibit a very weak intensity dependence of V_{oc} which is consistent with a close-to-optimal V_{bi}. The weak light intensity dependence of V_{oc} also has the advantage that the η of cells incorporating o-AuNC does not deteriorate at low light intensity (Figure 5).

A distinguishing feature of o-AuNC as a hole-extraction material in molecular OPV is their effectiveness at submonolayer surface coverage. It is also notable that the delay in the onset of the sharp rise in the forward dark current (Figures 3 and 4, insets), which is responsible for the increase in V_{oc}, is not accompanied by a statistically significant reduction in the reverse dark current, ruling out the possibility that the increase in V_{oc} results from a reduction in the reverse saturation current. These observations can be understood in terms of geometric enhancement of the electric field in the vicinity of the o-AuNC due to their high aspect ratio.[39] Geometric electric field enhancement is a well-documented phenomenon in the context of cold cathode field emission electron sources, although it has only recently been proposed to be operative in the context of organic optoelectronic devices.[40,41] The most appropriate model in the current context is that of a floating conducting sphere at the same potential as the underlying electrode,[39] with a separation equal to an OAm chain length. Using this model and correcting for the small anode−cathode separation in molecular OPV, one can estimate the electric field in the vicinity of the AuNC to be 3−4 times larger than that across the electrodes. In the current context this would amplify the role of the o-AuNC enhancing hole−*extraction* for $V < V_{bi}$ before abruptly switching to enhancing hole−*injection* for $V > V_{bi}$. The sharp knee in the forward dark current characteristics in both cell structures is evidence for such switching behavior. Furthermore, geometric electric field enhancement effects would not operate to reduce the reverse dark current which is also consistent with observation. More work to test this hypothesis is currently underway.

CONCLUSIONS

We have demonstrated a new strategy for dramatically increasing V_{oc} in molecular photovoltaics based on the incorporation of a submonolayer of surface oxidized AuNC at the ITO/donor interface. Crucially this nanomaterial is solution processed and activated for application in OPV using a simple oxidative treatment. This approach also reduces the cell-to-cell variability in V_{oc} by as much as 10-fold as compared to cells without o-AuNC and delivers superior performance to cells incorporating the archetypal hole-extraction layer PEDOT:PSS in high V_{oc} molecular OPV systems. The effectiveness of this nanomaterial for hole-extraction in small molecule OPV is interpreted in terms of the exceptionally high work function (~5.9 eV) and local electric field enhancement effects.

METHODS

OAm−AuNC Synthesis and Characterization. 190 mg of $HAuCl_4$ (Alfa Aesar) was dissolved in a 1:1 hexane/OAm mixture. The resulting complex is a rich orange color in appearance, indicative of the partial reduction of Au^0 from Au^{3+} to Au^{1+}. This solution is then added to a mixture of OAm (8 mL) and OA (10 mL) immediately prior to heating to 80 °C. Over the course of 5 h the reaction mixture changes from a pale, transparent yellow to a deep, opaque purple/red. Once cooled to room temperature the product was washed repeatedly in ethanol by centrifugation (8000 rpm, 10 min per cycle) with the supernatant discarded between each cycle and replaced with fresh ethanol. The dried product was redispersed in a known concentration of toluene. The size and shape distribution of the as-synthesized structures was determined using a JEOL 2000FX TEM. Dilute solutions were drop-cast onto a coated-Cu (300 mesh) grid for imaging.

Fabrication and Characterization of OPV. ITO glass substrates were cleaned *via* ultrasonication in (i) acetone, (ii) Decon Neutracon/H_2O, (iii) H_2O, and finally (iv) propan-2-ol. Hydrocarbon residue from the solvent was removed using UV/O_3 treatment. Submonolayer films of OAm−AuNC were spin-cast onto the treated substrates at 2000 rpm. All substrates, including references underwent a second UV/O_3 (Novascan PSD-UVT) treatment immediately prior to transfer into the vacuum system. UV/O_3 treatment involved exposure of the relevant substrates to UV light from a Hg lamp (185 and 254 nm, 20 mW/cm^2) at a distance of 25 mm from the substrate in a sealed air-filled chamber for 15 min followed by a 15 min incubation period.

OPV cells were fabricated under high vacuum (~10^{-7} mBar) using organic molecular beam deposition and thermal evaporation (Al cathodes). The photoactive organic materials; SubPc (Sigma Aldrich, 85%), ClAlPc (98%), and C_{60} (Nano-C Inc., 99.5%) were purified once by thermal gradient sublimation prior to deposition. SubPc, ClAlPc, C_{60}, and BCP were deposited at rates of 2, 1, 0.5, and 1 Å s^{-1}, respectively. Al cathodes were deposited *in situ* by evaporation through a shadow mask to give active device areas of 0.16 cm^{-2}. Device structures of anode/SubPc (140 Å)/C_{60} (325 Å)/BCP (80 Å)/Al (~1000 Å) or Anode/ClAlPc (200 Å)/ C_{60} (400 Å)/BCP (80 Å)/Al (~1000 Å) were fabricated, where the anode corresponds to either a UV/O_3-treated ITO glass

or UV/O_3-treated OAm−AuNC on ITO glass (*i.e.,* o-AuNC/ITO glass).

Current−voltage (J−V) characteristics were measured using a Keithley 2400 SourceMeter and Newport Solar Simulator. The light intensity was calibrated to AM1.5 solar illumination operating at 1 sun (100 mW cm^{-2}) using a series of optical cutoff filters (Thorlabs) and a PV Measurements Inc. calibrated silicon diode with KG5 color filter. Alterations to the optical cutoff filters selected allowed for a series of light intensity measurements. Incident photon to electron conversion efficiency (IPCE) measurements were obtained from the same light source coupled with a PTI monochromator. The monochromatic light intensity was calibrated with a Si photodiode (Thorlabs) and chopped at 500 Hz. Signal detection was performed with a current−voltage amplifier and lock-in amplifier.

Work Function Measurements (Kelvin Probe). All work function measurements were made in a nitrogen-filled glovebox using a Kelvin probe referenced to freshly cleaved highly oriented pyrolytic graphite (HOPG).

X-ray Photoelectron Spectroscopy (XPS). XPS spectra were recorded using a Kratos Axis Ultra spectrometer employing a monochromated Al Kα X-ray source ($h\nu$ = 1486.6 eV) and hemispherical energy analyzer. Survey scans were recorded at pass energy = 80 eV and high resolution scans at pass energy = 20 eV with the charge neutralized. All XPS spectra were processed in CasaXPS (version 2.3.15, standard Kratos sensitivity factors) and charge corrected with respect to the C 1s peak set to binding energy = 285 eV. Models were devised for Au 4f peaks based on summed Gaussian−Lorentzian (SGL) peak shapes with a Shirley background.

Acknowledgment. This work was supported by the UK Engineering and Physical Sciences Research Council (EPSRC) and the European Regional Development Fund/Advantage West Midlands Science City Materials Initiative (Project 2). R.A.H. is grateful to the Royal Academy of Engineering/EPSRC for the award of a Fellowship. We thank Prof. Tim Jones (University of Warwick) for access to his group facilities and Ms. Emily Smith (University of Nottingham) for assistance with the XPS data collection and analysis.

Supporting Information Available: Procedure for determining the oxide thickness at the surface of oxidized Au nanocrystals using XPS; additional figures. This material is available free of charge *via* the Internet at http://pubs.acs.org.

REFERENCES AND NOTES

1. Riede, M.; Mueller, T.; Tress, W.; Schueppel, R.; Leo, K. Small-Molecule Solar Cells—Status and Perspectives. *Nanotechnology* **2008**, *19*, 424001–424012.
2. Chen, H.; Hou, J.; Zhang, S.; Liang, Y.; Yang, G.; Yang, Y. Polymer Solar Cells with Enhanced Open-Circuit Voltage and Efficiency. *Nat. Photon.* **2009**, *3*, 649–653.
3. Gregg, B. A. The Photoconversion Mechanism of Excitonic Solar Cells. *MRS Bull.* **2005**, *30*, 20–22.
4. Tang, C. W. Two-Layer Organic Photovoltaic Cell. *Appl. Phys. Lett.* **1986**, *48*, 183–185.
5. Bailey-Salzman, R. F.; Rand, B. P.; Forrest, S. R. Near-Infrared Sensitive Small Molecule Organic Photovoltaic Cells Based on Chloroaluminum Phthalocyanine. *Appl. Phys. Lett.* **2007**, *91*, 013508−3.
6. Brumbach, M.; Placencia, D.; Armstrong, N. Titanyl Phthalocyanine/C_{60} Heterojunctions: Band-Edge Offsets and Photovoltaic Device Performance. *J. Phys. Chem. C* **2008**, *112*, 3142–3151.
7. Mutolo, K. L.; Mayo, E. I.; Rand, B. P.; Forrest, S. R.; Thompson, M. E. Enhanced Open-Circuit Voltage in Subphthalocyanine/C_{60} Organic Photovoltaic Cells. *J. Am. Chem. Soc.* **2006**, *128*, 8108–8109.
8. Hains, A. W.; Marks, T. J. High-Efficiency Hole Extraction/Electron-Blocking Layer to Replace Poly(3,4-ethylenedioxythiophene):Poly(styrene sulfonate) in Bulk-Heterojunction Polymer Solar Cells. *Appl. Phys. Lett.* **2008**, *92*, 023504.
9. Peumans, P.; Yakimov, A.; Forrest, S. R. Small Molecular Weight Organic Thin-Film Photodetectors and Solar Cells. *J. Appl. Phys.* **2003**, *93*, 3693–3723.
10. Ameri, T.; Dennler, G.; Lungenschmied, C.; Brabec, C. J. Organic Tandem Solar Cells: A Review. *Energy Environ. Sci.* **2009**, *2*, 347–363.
11. Potscavage, W. J.; Sharma, A.; Kippelen, B. Critical Interfaces in Organic Solar Cells and Their Influence on the Open-Circuit Voltage. *Acc. Chem. Res.* **2009**, *42*, 1758–1767.
12. Steim, R.; Kogler, F. R.; Brabec, C. J. Interface Materials for Organic Solar Cells. *J. Mater. Chem.* **2010**, *20*, 2499–2512.
13. Li, N.; Lassiter, B. E.; Lunt, R. R.; Wei, G.; Forrest, S. R. Open Circuit Voltage Enhancement Due to Reduced Dark Current in Small Molecule Photovoltaic Cells. *Appl. Phys. Lett.* **2009**, *94*, 023307.
14. Luo, J.; Wu, H.; He, C.; Li, A.; Yang, W.; Cao, Y. Enhanced Open-Circuit Voltage in Polymer Solar Cells. *Appl. Phys. Lett.* **2009**, *95*, 043301.
15. Sardar, R.; Funston, A. M.; Mulvaney, P.; Murray, R. W. Gold Nanoparticles: Past, Present, and Future. *Langmuir* **2009**, *25*, 13840–13851.
16. Chen, F.; Wu, J.; Lee, C.; Hong, Y.; Kuo, C.; Huang, M. H. Plasmonic-Enhanced Polymer Photovoltaic Devices Incorporating Solution-Processable Metal Nanoparticles. *Appl. Phys. Lett.* **2009**, *95*, 013305.
17. Lee, J. H.; Park, J. H.; Kim, J. S.; Lee, D. Y.; Cho, K. High Efficiency Polymer Solar Cells with Wet Deposited Plasmonic Gold Nanodots. *Org. Electron.* **2009**, *10*, 416–420.
18. Morfa, A. J.; Rowlen, K. L.; Reilly III, T. H.; Romero, M. J.; Van De Lagemaat, J. Plasmon-Enhanced Solar Energy Conversion in Organic Bulk Heterojunction Photovoltaics. *Appl. Phys. Lett.* **2008**, *92*, 13504.
19. Kumar, H.; Kumar, P.; Bhardwaj, R.; Sharma, G. D.; Chand, S.; Jain, S. C.; Kumar, V. Broad Spectral Sensitivity and Improved Efficiency in CuPc/Sub-Pc Organic Photovoltaic Devices. *J. Phys. D: Appl. Phys.* **2009**, *42*, 015103−3.
20. Cho, S. W.; Piper, L. F.; DeMasi, A.; Preston, A. R.; Smith, K. E.; Chauhan, K. V.; Sullivan, P.; Hatton, R. A.; Jones, T. S. Electronic Structure of C_{60}/Phthalocyanine/ITO Interfaces Studied Using Soft X-ray Spectroscopies. *J. Phys. Chem. C* **2010**, *114*, 1928–1933.
21. Wang, C.; Hu, Y. J.; Lieber, C. M.; Sun, S. H. Ultrathin Au Nanowires and Their Transport Properties. *J. Am. Chem. Soc.* **2008**, *130*, 8902–8903.
22. Peng, S.; Lee, Y.; Wang, C.; Yin, H.; Dai, S.; Sun, S. A Facile Synthesis of Monodisperse Au Nanoparticles and their Catalysis of CO Oxidation. *Nano Res.* **2008**, *1*, 229–234.
23. Sugiyama, K.; Ishii, H.; Ouchi, Y.; Seki, K. Dependence of Indium−Tin-Oxide Work Function on Surface Cleaning Method as Studied by Ultraviolet and X-ray Photoemission Spectroscopies. *J. Appl. Phys.* **2000**, *87*, 95–298.
24. Pang, S.; Kurosawa, Y.; Kondo, T.; Kawai, T. Decomposition of Monolayer Coverage on Gold Nanoparticles by UV/Ozone Treatment. *Chem. Lett.* **2005**, *34*, 544–545.
25. King, D. E. Oxidation of Gold by Ultraviolet Light and Ozone at 25°C. *J. Vac. Sci., Technol. A* **1995**, *13*, 1247–1253.
26. Irissou, E. Gold Oxide Thin Film Grown by Pulsed Laser Deposition in an O_2 Atmosphere. *Thin Solid Films* **2005**, *472*, 49–57.
27. Rentenberger, S.; Vollmer, A.; Zojer, E.; Schennach, R.; Koch, N. UV/Ozone Treated Au for Air-Stable, Low Hole Injection Barrier Electrodes in Organic Electronics. *J. Appl. Phys. 2006* **2006**, *100*, 053701.
28. Boyen, H. G.; Kästle, G.; Weigl, F.; Koslowski, B.; Dietrich, C.; Ziemann, P.; Spatz, J. P.; Riethmüller, S.; Hartmann, C.; Möller, M.; *et al.* Oxidation-Resistant Gold-55 Clusters. *Science* **2002**, *297*, 1533–1536.
29. Shard, A. G.; Wang, J.; Spencer, S. J. XPS Topofactors: Determining Overlayer Thickness on Particles and Fibres. *Surf. Interface Anal.* **2009**, *41*, 541–548.
30. Kim, W.; Lee, J. Effect of Oxygen Plasma Treatment on Reduction of Contact Resistivity at Pentacene/Au Interface. *Appl. Phys. Lett.* **2006**, *88*, 262102.
31. Stadlober, B.; Haas, U.; Gold, H.; Haase, a.; Jakopic, G.;

Leising, G.; Koch, N.; Rentenberger, S.; Zojer, E. Orders-of-Magnitude Reduction of the Contact Resistance in Short-Channel Hot Embossed Organic Thin Film Transistors by Oxidative Treatment of Au-Electrodes. *Adv. Funct. Mater.* **2007**, *17*, 2687–2692.
32. Lin, Y.; Chu, J.; Su, Y.; Lee, C.; Chang, H. Improved Ohmic Contacts on Pentacene based on Au with Ultraviolet Irradiation Treatment. *Thin Solid Films* **2010**, *518*, 2707–2709.
33. Plieth, W. The Work Function of Small Metal Particles and Its Relation to Electrochemical Properties. *Surf. Sci.* **1985**, *156*, 530–535.
34. Schnippering, M.; Carrara, M.; Foelske, A.; Kötz, R.; Fermín, D. J. Electronic Properties of Ag Nanoparticle Arrays. A Kelvin Probe and High Resolution XPS Study. *Phys. Chem. Chem. Phys.* **2007**, *9*, 725–730.
35. Perez, M. D.; Borek, C.; Forrest, S. R.; Thompson, M. E. Molecular and Morphological Influences on the Open Circuit Voltages of Organic Photovoltaic Devices. *J. Am. Chem. Soc.* **2009**, *131*, 9281–9286.
36. Barker, J. A.; Greenham, N. C.; Ramsdale, C. M. Modeling the Current−Voltage Characteristics of Bilayer Polymer Photovoltaic Devices. *Phys. Rev. B* **200**, *67*, 075205.
37. Ramsdale, C. M.; Barker, J. A.; Arias, A. C.; Mackenzie, J. D.; Friend, R. H.; Greenham, N. C. The Origin of the Open Circuit Voltage in Polyfluorene-Based Photovoltaic Devices. *J. Appl. Phys.* **2002**, *92*, 4266–4270.
38. Braun, S.; Salaneck, W. R.; Fahlman, M. Energy-Level Alignment at Organic/Metal and Organic/Organic Interfaces. *Adv. Mater.* **2009**, *21*, 1450–1472.
39. Forbes, R. G.; Edgcombe, C. J.; Valdrè, U. Some Comments on Models for Field Enhancement. *Ultramicroscopy* **2003**, *95*, 57–65.
40. Liu, D.; Fina, M.; Guo, J.; Chen, X.; Liu, G.; Johnson, S. G.; Mao, S. S. Organic Light-Emitting Diodes with Carbon Nanotube Cathode−Organic Interface Layer. *Appl. Phys. Lett.* **2009**, *94*, 013110.
41. Miller, A. J.; Hatton, R. A.; Silva, S. R. Interpenetrating Multiwall Carbon Nanotube Electrodes for Organic Solar Cells. *Appl. Phys. Lett.* **2006**, *89*, 133117.